Exciton Photophysics of Carbon Nanotubes

Mildred S. Dresselhaus,[1] Gene Dresselhaus,[2] Riichiro Saito,[3] and Ado Jorio[4]

[1]Department of Electrical Engineering and Computer Science and Department of Physics, [2]Francis Bitter Magnet Laboratory, Massachusetts Institute of Technology, Cambridge, Massachusetts 02139-4307; email: millie@mgm.mit.edu, gene@mgm.mit.edu

[3]Department of Physics, Tohoku University and CREST, JST, Sendai 980-8578, Japan; email: rsaito@flex.phys.tohoku.ac.jp

[4]Departamento de Física, Universidade Federal de Minas Gerais, Belo Horizonte - MG 30123-970, Brazil; email: adojorio@fisica.ufmg.br

Annu. Rev. Phys. Chem. 2007. 58:719–47

First published online as a Review in Advance on January 2, 2007

The *Annual Review of Physical Chemistry* is online at http://physchem.annualreviews.org

This article's doi: 10.1146/annurev.physchem.58.032806.104628

0066-426X/07/0505-0719$20.00

Key Words

photoluminescence, resonance Raman spectroscopy, Bethe-Salpeter equation, dark exciton, phonon side band, ratio problem

Abstract

The goal of this chapter is to review the importance of excitons to single-wall carbon nanotube (SWNT) optics. We have developed the presentation for both researchers in the SWNT field who want to learn more about the unusual aspects of SWNT exciton photophysics and researchers more knowledgeable about the physics of excitons, but not about SWNT physics. Excitons in SWNTs are special because graphite has two energy bands at the Fermi energy related to time-reversal symmetry and because SWNTs are actually one dimensional. This review discusses both theoretical and experimental points of view, thus aiming to provide a summary of the most important work in the field, as well as to identify open questions.

1. INTRODUCTION

SWNTs: single-wall carbon nanotubes

Many-body effects: electron-electron Coulomb repulsion and electron-hole Coulomb attraction, which relate to the electron self-energy and exciton binding energy, respectively

Exciton: an excited state formed by the Coulomb binding of an excited electron to a hole

BZ: Brillouin zone

Single-wall carbon nanotubes (SWNTs) represent one of the best known materials for the study of exciton photophysics, both from a theoretical and experimental viewpoint. SWNTs are reasonably cheap and commonly available materials, so they are accessible to almost all experimental groups. They involve only carbon atoms, and hence theoretical calculations can be carried out using a relatively simple model Hamiltonian.

The one-dimensional (1D) aspect of SWNTs gives further simplification to the theoretical modeling, as well as a strong increase in the importance of excitonic effects. The optical transition energies in SWNTs sensitive to these excitonic effects have been studied in detail through fluorescence and Raman spectroscopy experiments (1–3). Although some aspects of the experiments can be interpreted within the context of a simple, noninteracting electron model (4, 5), it has become increasingly clear that electron-electron interactions also play an important role in determining the optical transition energies. Moreover, both theoretical calculations and experimental measurements show that the exciton binding energies are anomalously large in carbon nanotubes, corresponding to a substantial fraction of the band gap, thus indicating the importance of many-body effects in this quasi-1D system (6–10). Researchers have made rapid progress in this field, and this seems like an opportune time to review our present understanding of the magnitudes and dependencies of the exciton effects.

This review begins with an overview of the exciton physics (Section 2), briefly addressing the general properties of excitons, but also emphasizing the uniqueness of excitons in graphite and SWNTs. The unusual geometrical structure of sp^2 carbons to which these materials relate gives rise to two special points in the Brillouin zone (BZ) (namely K and K'), which are related by time-reversal symmetry (2), making these sp^2 carbon systems different from other nano systems, which also have large excitonic effects, but do not have similar symmetry constraints. Differences in symmetry are important and guide electronic-structure calculations and the interpretation of experiments. Therefore, an analysis of exciton symmetries in SWNTs is needed to understand in greater detail many aspects of their optical properties.

From a theoretical point of view, Ando (6) introduced early on the importance of excitons to SWNTs by studying the excitations of nanotubes within a static screened Hartree-Fock approximation. Later on, after experimental results started to show the importance of excitons, detailed first-principles calculations of the effects of many-body interactions on the optical properties were performed for nanotubes with very small diameter (d_t) (7, 8, 11, 12), and some descriptions of excitons in nanotubes based on simpler or different models (13–16) were also developed. However, a systematic dependence of exciton effects (including wave function–related phenomena) on the nanotube diameter and chiral angle (presented in Section 3) has only recently been developed (17, 18), and these results are important for discussing the photophysical properties of SWNTs.

In Section 4, we present experimental evidence for excitons in SWNTs. The importance of many-body effects in the form of excitonic electron-hole attraction and Coulombic electron-electron repulsion in SWNTs was first brought into sharp focus

experimentally in the context of the so-called ratio problem (1, 19). Subsequently, other experimental results, such as the two-photon absorption experiments (9, 10) and the lineshape analysis of exciton-phonon side bands (20), provided strong evidence for the excitonic nature of the lower energy transition (E_{11}^S). We begin this section by discussing the historically important ratio problem, followed by more definitive experimental evidence for excitons coming from two-photon absorption and phonon side band experiments. This is followed by discussions of the exciton binding energy and the interesting p/d_t scaling law for the various E_{ii} levels. Finally we address the importance of dark excitons and present interesting results on electro-optical effects. We emphasize the interplay between experiment and theory in establishing the role of excitons in the photophysics of carbon nanotubes and in gaining an understanding of the observed phenomena. The review concludes in Section 5 with a summary and an outlook toward open issues.

Ratio problem: relates to the ratio between the second and first optical transition energies not being equal to two in semiconducting SWNTs

Two-photon absorption: the use of fast-optics high-intensity light pulses, which allows two photons to be absorbed before emission occurs

Exciton side band: exciton-phonon complex that behaves as a single quantum entity

Dark exciton: exciton that cannot be observed optically

PL: photoluminescence

2. OVERVIEW

An exciton consists of a photo-excited electron and a hole bound to each other by a Coulomb interaction in a semiconducting material. In many commonly occurring semiconductors (such as Si, Ge, and III-V compounds), we can calculate the binding energy of an exciton in three-dimensional materials by a hydrogenic model with a reduced effective mass and a dielectric constant, giving a binding energy on the order of ~10 meV, with discrete levels below the single-particle excitation spectra. Thus optical absorption to exciton levels is usually observed only at low temperatures. However, in an SWNT, because of its 1D properties, the electron-hole attraction energy becomes larger and can be as large as 1 eV, so exciton effects can be observed at room temperature. Thus excitons are essential for explaining optical processes in SWNTs, such as optical absorption, photoluminescence (PL), and resonance Raman spectroscopy.

2.1. The Exciton Wave Vector

A single-particle picture of carriers is simple and easy to understand. In a semiconducting material, an electron can be excited from the valence to the conduction energy band, by gaining more than the band gap energy of the material. The energy difference E_{ii} for an optical transition between i-th valence and i-th conduction bands on a one-electron picture is directly related to the excitation energy. An excitonic picture, however, cannot be represented by a single-particle model, and we cannot generally use the energy-dispersion relations directly to obtain the excitation energy for the exciton. If the electron and hole wave functions are localized in the same spatial region, the attractive Coulomb interaction between the electron and hole increases the binding energy, while the kinetic energy and the Coulomb repulsion between the electrons become large, too. Thus the optimum localized distance determines the exciton binding energy. The screening of the attractive Coulomb interaction by other conduction electrons is the reason why excitons usually are not important in

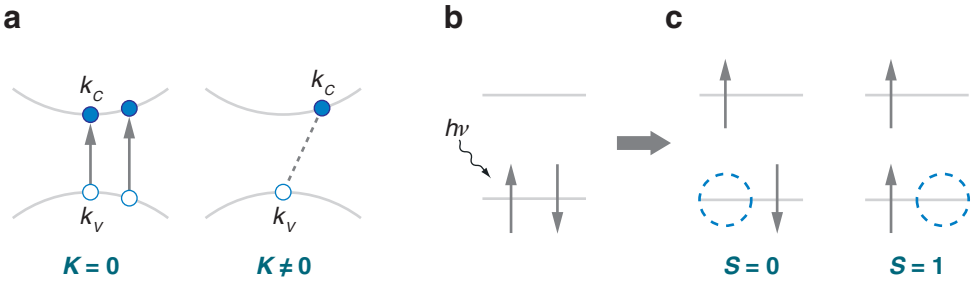

Figure 1

(*a*) A singlet exciton formed at $K = 0$ in a crystal, where $k_c = k_v$ (*left*), at either the band extremum or away from the band extremum. If $k_c \neq k_v$, $K \neq 0$, giving rise to a dark exciton (*right*). (*b*) When a photon is absorbed by an electron with spin ↑ (*left*), we get a singlet exciton ($S = 0$, *right*). If the spin of the electron is ↑, we here define the spin of the hole left behind as ↓ . (*c*) A triplet exciton ($S = 1$) that is a dark exciton.

metals. The repulsive Coulomb interaction between two electrons causes the wave vector k for an excited electron to no longer be a good quantum number.

Because the exciton wave function is localized in real space, the exciton wave function in k space is a linear combination of Bloch wave functions with different k states. Thus the definition of k_c and k_v may not be so clear. However, because the exciton wave function is localized in k space, as well,[1] we can define k_c or k_v as the central position of the corresponding wave functions in k space.

When we consider an optical transition in a crystal, we expect a vertical transition, $k_c = k_v$ (**Figure 1*a***), where k_c and k_v are the wave vectors of the electron and hole, respectively. The wave vector of the center of mass for the exciton is defined by $K = (k_c - k_v)/2$, whereas the relative coordinate is defined by $k = k_c + k_v$, in which the hole (created by exciting an electron) has the opposite sign for its wave vector and effective mass as compared with the electron. The exciton has an energy dispersion as a function of K, which represents the translational motion of an exciton. Thus only the $K = 0$ exciton can recombine by emitting a photon. Correspondingly, a $K \neq 0$ exciton cannot recombine directly to emit a photon and therefore is a dark exciton. Recombination emission for $K \neq 0$ is, however, possible by a phonon-assisted process, which we call an indirect transition.

2.2. The Exciton Spin

When we discuss the interaction between an electron and a hole, the definition of the total spin for an exciton is a bit different from the conventional idea of two electrons in a molecule (or a crystal). A hole is a different particle from an electron, but, nevertheless, an exchange interaction between the electron and the hole exists, just like for two electrons in a hydrogen molecule.

[1] Imagine that the exciton wave function is a Gaussian function. The Fourier transformation of a Gaussian in real space is a Gaussian in k space, too.

When an electron absorbs a photon, an electron with spin ↑, for example, is excited to an excited state (**Figure 1*b***), leaving behind a hole at the energy level at which the electron with up-spin had previously been. This hole has not only a wave vector of $-k$ and an effective mass of $-m^*$ (as mentioned in Section 2.1), but also is defined to be in a spin-down hole state. The exciton thus obtained (**Figure 1*b***) is called a spin singlet, with $S = 0$, because the definition of S for the two-level model shown here is in terms of the two actual electrons present,[2] and in this sense the definition for the two actual electrons and the definition for the $S = 0$ exciton are identical. We note that **Figure 1*b*** does not represent an $S = 0$ eigenstate. To make an eigenstate, we must take the antisymmetric combination of the state shown in **Figure 1*b*** with an electron ↓ and hole ↑ (21). In contrast, a triplet exciton ($S = 1$) can be represented by two electrons, one in the ground state and the other in an excited state to give a total spin of $S = 1$ (**Figure 1*c***).[3] For the triplet state in **Figure 1*c***, we define the hole to have a spin ↑, and the resulting state shown is an eigenstate ($m_s = 1$) for $S = 1$. A triplet exciton cannot be recombined by emitting a photon because of the Pauli principle. We call such an exciton a dark exciton.[4] An exchange interaction between a hole and an electron works only for $S = 0$ (see **Figure 1*b***), and thus the $S = 1$ state in **Figure 1*c*** has a lower energy than the $S = 0$ state (see also Equation 2 in Section 3.1). For the more familiar case of just two electrons, the exchange interaction works for the $S = 1$ case, and therefore the $S = 1$ state lies lower in energy than the $S = 0$ state.

Bright exciton: exciton that can be observed optically

2.3. Uniqueness of the Exciton in Graphite and Single-Wall Carbon Nanotubes

The electronic structure of an SWNT and graphite is unique insofar as there are two inequivalent energy bands near the two hexagonal corners K and K' of the BZ. We therefore distinguish the regions around K and K' from one another and call them the two valleys of SWNTs and graphite. Although an optical transition occurs vertically in k space, we can consider the electron and the hole in the electron-hole pair to be either in the same valley, or an electron to be in one valley and a hole in the other valley. The latter pair can form an excitonic state, but it never recombines radiatively because the electron and hole do not exist in the same valley; we call such a state a dark exciton. In addition to the conventional bright exciton (an electron-hole pair from the same valley that recombines radiatively[5]), the coexistence of many different types of excitons is important for understanding the optical properties of SWNTs.

In resonance Raman spectra, PL, or Rayleigh scattering, we can observe a signal even from a single SWNT molecule. In a one-particle picture of optical processes,

[2] The electric dipole transition does not change the total spin of the ground state, which is $S = 0$.

[3] The reader should not be confused by having $S = 1$ for the triplet state because the two spin-up electrons are in different energy states.

[4] A magnetic field could flip a spin and lead to the recombination of the triplet exciton.

[5] Even within the same valley, one of the two possible exciton types is a dark exciton because of symmetry requirements (22, 23).

VHS: van Hove singularity

Bethe-Salpeter equation: equation for solving for the exciton energy and wave function

a strong enhancement of the optical intensities can be understood in terms of the 1D van Hove singularities (VHSs) in the joint density of states connecting the valence and conduction energy bands. In an excitonic picture, an exciton has an energy dispersion as a function of the center-of-mass wave vector, and we expect 1D VHSs in the excitonic density of states from the ground states, at which optical absorption becomes strong, and this occurs when the center-of-mass wave vector vanishes. The assignment of the excitation energy to an SWNT with (n, m) indices works well by interpreting the one-particle picture in terms of the exciton VHS position. This exciton-energy position can be modified by changing the surrounding materials by the use of substrates, solutions, or wrapping agents (environmental effects) in the space surrounding an SWNT or by electrochemical doping.

3. THEORY FOR EXCITONS IN CARBON NANOTUBES

3.1. Bethe-Salpeter Equation

Next we show how to calculate the exciton energy Ω_n and wave function Ψ^n based on a solid-state physics approach (6, 7, 17, 24–28). Because the exciton wave function is localized in real space by a Coulomb interaction, the wave vector of an electron ($\mathbf{k}_c$) or a hole ($\mathbf{k}_v$) is not a good quantum number any more, and thus the exciton wave function Ψ_n for the n-th exciton energy Ω_n is given by a linear combination of Bloch functions at many $\mathbf{k}_c$ and $\mathbf{k}_v$ wave vectors. We obtain the mixing of different wave vectors by the Coulomb interaction by the so-called Bethe-Salpeter equation:

$$\sum_{\mathbf{k}_c\mathbf{k}_v}\{[E(\mathbf{k}_c) - E(\mathbf{k}_v)]\delta_{\mathbf{k}'_c\mathbf{k}_c}\delta_{\mathbf{k}'_v\mathbf{k}_v} + K(\mathbf{k}'_c\mathbf{k}'_v, \mathbf{k}_c\mathbf{k}_v)\}\Psi^n(\mathbf{k}_c\mathbf{k}_v) = \Omega_n\Psi^n(\mathbf{k}'_c\mathbf{k}'_v), \qquad (1)$$

where $E(\mathbf{k}_c)$ and $E(\mathbf{k}_v)$ are the quasi-electron and quasi-hole energies, respectively. Here quasi-particle means that we add a Coulomb interaction to the one-particle energy and that the particle has a finite lifetime. Equation 1 represents simultaneous equations for many $\mathbf{k}'_c$ and $\mathbf{k}'_v$ points.

Here Ω_n is the energy of the n-th excitation, and Ψ^n $(\mathbf{k}_c\mathbf{k}_v)$ are the components of the excitonic wave functions. The mixing term of Equation 1, which we call the kernel, K $(\mathbf{k}'_c\mathbf{k}'_v, \mathbf{k}_c\mathbf{k}_v)$ is given by

$$K(\mathbf{k}'_c\mathbf{k}'_v, \mathbf{k}_c\mathbf{k}_v) = -K^{\mathrm{d}}(\mathbf{k}'_c\mathbf{k}'_v, \mathbf{k}_c\mathbf{k}_v) + 2\delta_S K^{\mathrm{x}}(\mathbf{k}'_c\mathbf{k}'_v, \mathbf{k}_c\mathbf{k}_v), \qquad (2)$$

with $\delta_S = 1$ for spin-singlet and 0 for spin-triplet states (see Section 2.2). The direct and exchange interaction kernels K^{d} and K^{x} are given by the following integrals (21):

$$\begin{aligned} K^{\mathrm{d}}(\mathbf{k}'_c\mathbf{k}'_v, \mathbf{k}_c\mathbf{k}_v) &\equiv W(\mathbf{k}'_c\mathbf{k}_c, \mathbf{k}'_v\mathbf{k}_v) \\ &= \int d\mathbf{r}'d\mathbf{r}\psi^*_{\mathbf{k}'_c}(\mathbf{r}')\psi_{\mathbf{k}_c}(\mathbf{r}')w(\mathbf{r}', \mathbf{r})\psi_{\mathbf{k}'_v}(\mathbf{r})\psi^*_{\mathbf{k}_v}(\mathbf{r}), \qquad (3) \\ K^{\mathrm{x}}(\mathbf{k}'_c\mathbf{k}'_v, \mathbf{k}_c\mathbf{k}_v) &= \int d\mathbf{r}'d\mathbf{r}\psi^*_{\mathbf{k}'_c}(\mathbf{r}')\psi_{\mathbf{k}'_v}(\mathbf{r}')v(\mathbf{r}', \mathbf{r})\psi_{\mathbf{k}_c}(\mathbf{r})\psi^*_{\mathbf{k}_v}(\mathbf{r}), \end{aligned}$$

where w and v are the screened and bare Coulomb potentials, respectively, and ψ is the quasi-particle eigenfunction as discussed below.

The quasi-particle energies are the sum of the single-particle energy [$\varepsilon(\mathbf{k})$] and self-energy [$\Sigma(\mathbf{k})$]:

$$E(\mathbf{k}_i) = \varepsilon(\mathbf{k}_i) + \Sigma(\mathbf{k}_i), \quad (i = \mathrm{c}, \mathrm{v}), \tag{4}$$

ETB: extended tight binding

where $\Sigma(\mathbf{k})$ is expressed by

$$\Sigma(\mathbf{k}_c) = -\sum_{q} W(\mathbf{k}_c(\mathbf{k}+\mathbf{q})_v, (\mathbf{k}+\mathbf{q})_v\mathbf{k}_c),$$
$$\Sigma(\mathbf{k}_v) = -\sum_{q} W(\mathbf{k}_v(\mathbf{k}+\mathbf{q})_v, (\mathbf{k}+\mathbf{q})_v\mathbf{k}_v). \tag{5}$$

To obtain the kernel and self-energy, we obtain the single-particle Bloch wave function $\psi_{\mathbf{k}}(\mathbf{r})$ and screening potential W by either a first-principles calculation (7) or an extended tight-binding (ETB) wave function and a random-phase-approximation calculation (17). In the random-phase approximation, the static screened Coulomb interaction is expressed by $W = V/\kappa\varepsilon(\mathbf{q})$, with a static dielectric constant κ and the dielectric function $\varepsilon(\mathbf{q}) = 1 + v(\mathbf{q})\Pi(\mathbf{q})$. By calculating the polarization function $\Pi(\mathbf{q})$ and Fourier transformation of the unscreened Coulomb potential $v(\mathbf{q})$, we get information, which is sufficient for describing the exciton energy and wave function (6, 17). For 1D materials, the Ohno potential is commonly used for the unscreened Coulomb potential v for π-orbitals (13):

$$v(|\mathbf{R}_{u's'} - \mathbf{R}_{0s}|) = \frac{U}{\sqrt{\left(\frac{4\pi\varepsilon_0}{e^2}U|\mathbf{R}_{us} - \mathbf{R}_{0s'}|\right)^2 + 1}}, \tag{6}$$

where U is the energy cost to place two electrons on a single site ($|\mathbf{R}_{us} - \mathbf{R}_{s'}| = 0$) and is taken as $U \equiv U_{\pi_a\pi_a\pi_a\pi_a} = 11.3$ eV for π-orbitals (13).

3.2. Exciton Energy Dispersion

For an electron-hole pair, we introduce wave vectors for the center-of-mass $\mathbf{K}$ and relative motion $\mathbf{k}$:

$$\mathbf{K} = (\mathbf{k}_c - \mathbf{k}_v)/2, \quad \mathbf{k} = \mathbf{k}_c + \mathbf{k}_v. \tag{7}$$

The Bethe-Salpeter equation (Equation 1) is rewritten in terms of $\mathbf{K}$ and $\mathbf{k}$. Because the Coulomb interaction is related to the relative coordinate of an electron and a hole, the center-of-mass motion $\mathbf{K}$ can be treated as a good quantum number.[6] Thus the exciton energy is given by an energy dispersion as a function of $\mathbf{K}$.

In **Figure 2**, we show the two-dimensional (2D) BZ of graphite and the cutting lines for a (6, 5) single-wall nanotube. Because optical transitions occur around the K or K' points in the 2D BZ, we can expect four possible combinations of an electron and hole pair (**Figure 2**) (23). The excitons in an SWNT can then be classified according to their $2\mathbf{K}$ value. If both the electron ($\mathbf{k}_c$) and hole ($\mathbf{k}_v$) are from the K (or K') region, then $2\mathbf{K} = \mathbf{k}_c - \mathbf{k}_v$ lies in the Γ region, and the corresponding exciton is an $A_{1,2}$ symmetry exciton (23). If an electron is from the K region and a hole is

[6] Strictly speaking, when we consider the screening effect of an exciton by other electrons, $\mathbf{K}$ is no longer a good quantum number.

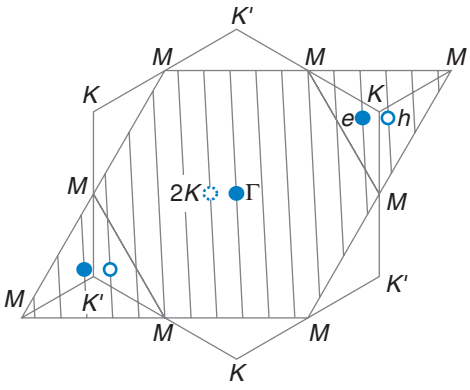

Figure 2

The three inequivalent regions in the two-dimensional Brillouin zone (2D BZ) of graphite. The cutting lines (Section 3.1) for a (6, 5) single-wall carbon nanotube (SWNT) are shown. The electron-hole pairs [at a *solid circle* near K (or K')] and the corresponding center-of-mass momentum $2\mathbf{K} = \mathbf{k}_c - \mathbf{k}_v$ (*solid circle* at Γ) for an $A_{1,2}$ exciton of the (6, 5) SWNT are indicated. The electron-hole pair with the electron and hole lying on the second and first cutting lines to the K point and the electron-hole pair with the electron and hole lying on the first and second cutting lines to the K' point correspond to an E_{12} exciton with the center-of-mass momentum 2K (*dotted circle* near the Γ point) on the first cutting line to the Γ point (17).

from the K' region, their $2\mathbf{K}$ lies in the K region, and this exciton is an E symmetry exciton. If an electron is from the K' region and a hole is from the K region, their $2\mathbf{K}$ lies in the K' region, and this exciton is an E^* symmetry exciton.

For A-symmetry excitons, the electron-hole pair $|\mathbf{k}_c, \mathbf{k}_v\rangle = |\mathbf{k}, \mathbf{K}\rangle$ with the electron and hole from the K region, and $|-\mathbf{k}_v, -\mathbf{k}_c\rangle = |-\mathbf{k}, \mathbf{K}\rangle$ with the electron and hole from the K' region having the same magnitude for $\mathbf{K}$. Thus we can recombine these two electron-hole pairs to get

$$A_{2,1} = |\mathbf{k}, \pm, \mathbf{K}\rangle = \frac{1}{\sqrt{2}}(|\mathbf{k}, \mathbf{K}\rangle \pm |-\mathbf{k}, \mathbf{K}\rangle). \quad (8)$$

Here $|\mathbf{k}, +, \mathbf{K}\rangle$ and $|\mathbf{k}, -, \mathbf{K}\rangle$ are antisymmetric (A_2) and symmetric (A_1), respectively, under the C_2 rotation around the axis perpendicular to the nanotube axis (22).

3.3. Exciton Wave Functions

In this section we discuss mainly the calculated results on bright excitons reported by Jiang et al. (17). In **Figure 3**, we plot the energy dispersion of $E_{ii}(A_j)$ ($i = 1, 2, j = 1, 2$) excitons with spin $S = 0, 1$ for a (6, 5) SWNT, where E_{ii} denotes the energy separation of the i-th valence band to the i-th conduction band. We use the same notation of E_{ii} for the exciton (29), too, for simplicity. The exciton with the largest energy dispersion shows a parabolic energy-dispersion relation, which reflects the free particle of an exciton with a mass. For A_1 excitons, $S = 0$ and $S = 1$ are degenerate because the exchange interaction vanishes by symmetry. **Figure 3*d*** gives the excitation energy levels for $K = 0$ $E_{11}(A^v)$ states. For spin $S = 0$ states,

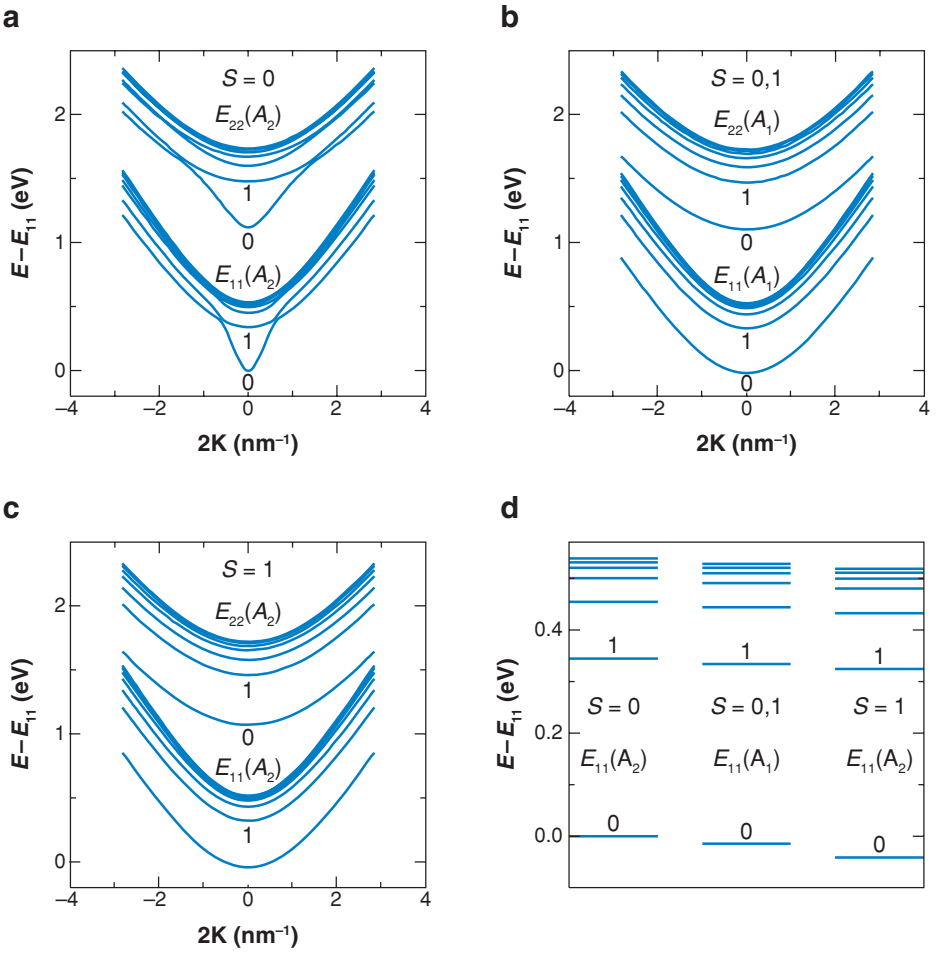

Figure 3

The excitation energy dispersions for (*a*) $E_{11}(A_2)$ ($S = 0$) and $E_{22}(A_2)$ ($S = 0$), (*b*) $E_{11}(A_1)$ ($S = 0, 1$) and $E_{22}(A_1)$ ($S = 0, 1$), and (*c*) $E_{11}(A_2)$ ($S = 1$) and $E_{22}(A_2)$ ($S = 1$) excitons for a (6, 5) single-wall carbon nanotube (SWNT). The excitation energy levels for $\bar{K} = 0$ excitons are also shown in *d* (17).

$E_{11}(A_2^0)$ has a somewhat larger energy than $E_{11}(A_1^0)$. This means that the bright A_2 exciton is not the lowest energy state, in agreement with the work of others (30). The Coulomb energy $K^{\mathrm{d}}(\mathbf{k}', -\mathbf{k}; \pm, \mathbf{K})$, which is the energy for an intervalley scattering process, thus has a one order of magnitude smaller energy than the corresponding energy for an intravalley scattering process, $K^{\mathrm{d}}(\mathbf{k}', \mathbf{k}; \pm, \mathbf{K})$. Therefore, the energy difference between $E_{11}(A_2^0)$ and $E_{11}(A_1^0)$ (for $S = 0$) is predicted and measured to be quite small (approximately 12 meV in **Figure 3*d***). Moreover, in **Figure 3*d*** the triplet $E_{11}(A_2^0)$ state lies approximately 35 meV below the singlet $E_{11}(A_2^0)$ state. The energy difference between the triplet and singlet $E_{11}(A_2)$ states is determined by the

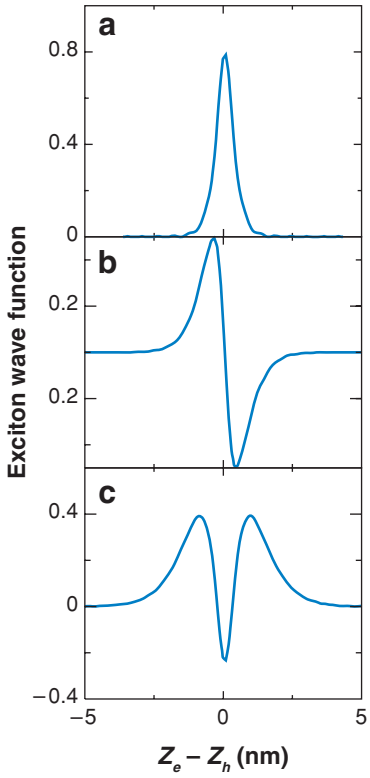

Figure 4

The magnitude of the exciton wave functions along the nanotube axis of an (8, 0) single-wall carbon nanotube (SWNT) for the states (*a*) $E_{22}(A_2^0)$, (*b*) $E_{22}(A_2^1)$, and (*c*) $E_{22}(A_2^2)$ (17).

exchange Coulomb interaction, $K^{\mathrm{x}}(\mathbf{k}', \mathbf{k}; \mathbf{K})$ (see Equation 3), which is approximately one order of magnitude smaller than the direct Coulomb interaction $K^{\mathrm{d}}(\mathbf{k}', \mathbf{k}; \mathbf{K})$ in SWNTs. The energy difference between the singlet $E_{11}(A_2^0)$ state, and $E_{11}(A_1^0)$ state, and the energy difference between the singlet and triplet $E_{11}(A_2^0)$ states are consistent with those found by previous calculations (11, 14). Hereafter, we mainly discuss the singlet bright exciton $E_{ii}(A_2^0)$ states with $K = 0$.

In **Figure 4** we show the exciton wave functions along the nanotube axis of an (8, 0) SWNT for several of the $E_{22}(A_2^\nu)$ states with lower excitation energies and with $\nu = 0$, 1, and 2 (17). Because of the orthogonalization of the wave functions, we can see wave functions with 0, 1, 2 nodes for **Figures 4*a*,*b*,*c***, respectively. The localization of the wave function for $E_{22}(A_2^0)$ for the (8, 0) SWNT is approximately 1 nm at full width at half-maximum. The localization length increases with increasing energy and with increasing nanotube diameter, reflecting the change from one dimension to two.

In an SWNT or graphite, there are two sublattices, *A* and *B*. For $E_{22}(A_2^0)$ and $E_{22}(A_2^2)$, the wave function has a similar amplitude for the *A* and *B* sublattices, whereas for $E_{22}(A_2^1)$, the amplitude of the wave function of the electron and hole occupies one

of the two sublattices exclusively. The latter behavior of the wave function (that the amplitude of the wave function can exist only on one sublattice) can be seen for localized edge states. Thus we expect an interesting behavior to occur when the exciton becomes localized at the end of an SWNT.

The $E_{22}(A_2^0)$ and $E_{22}(A_2^2)$ excitons are symmetric, and the $E_{22}(A_2^1)$ exciton is antisymmetric on reflection about the z axis. It then follows that the $E_{22}(A_2^0)$ and $E_{22}(A_2^2)$ excitons are bright and the $E_{22}(A_2^1)$ exciton is dark with respect to linearly polarized light parallel to the z axis. In the two-photon absorption experiments, the $E_{22}(A_2^2)$ exciton becomes bright (9). For an achiral (armchair or zigzag) SWNT, exciton wave functions are either even or odd functions of z because of the inversion center in the SWNT. Thus we use A_{2u} or A_{2g} to label $E_{22}(A_2^1)$ or $E_{22}(A_2^0)$ [and $E_{22}(A_2^2)$], respectively, for achiral SWNTs (23).

The localized exciton wave function is constructed by mixing many k states in which the mixing coefficients are determined by the Bethe-Salpeter equation (Equation 1). We show above that the envelope functions for the three wave functions given in **Figure 4** can be fitted to a Gaussian [e^{-Cz^2}, ze^{Cz^2}, and $(Az^2 - B)e^{Cz^2}$], respectively. The mixing coefficients (Fourier transformation) are also localized in k space around one-particle k points for a given E_{ii}, and this localization is described by a wave function full-width at half-maximum magnitude ℓ_k.

In **Figure 5**, we plot ℓ_k in the 1D k space for the bright exciton states, $E_{11}(A_2^0)$ and $E_{22}(A_2^0)$, and for all SWNTs with diameter (d_t) in the range of 0.5 mn $< d_t <$ 1.6 nm. In the figure, we also plot the cutting line spacing $2/d_t$ by the solid line. An important message here is that ℓ_k is smaller than $2/d_t$ for all SWNTs. This result indicates that one cutting line is sufficient to describe individual $E_{ii}(A)$ states. Consequently, the calculation for the Bethe-Salpeter equation is reduced significantly for the case of carbon nanotubes. For the higher energy states—$E_{ii}(A_2^\nu)$ states with $\nu = 1, 2, \cdots$—the ℓ_k values are smaller than that for $E_{ii}(A_2^0)$ because the wave functions for $E_{ii}(A_2^\nu)$ are more delocalized in real space. Generally, the i-th cutting line is sufficient to describe $E_{ii}(A)$, E_{ii}(E), and E_{ii}(E*) states,[7] and the i-th and $(i + 1)$-th cutting lines are sufficient to describe $E_{ii+1}(A)$ and $E_{i+1i}(A)$ states. Because metallic SWNTs (M-SWNTs) have smaller ℓ_k than semiconducting SWNTs (S-SWNTs), the above conclusion is also valid for M-SWNTs.

The assumption that we consider only one cutting line is valid so long as the range of the Coulomb interaction is larger than the diameter d_t of an SWNT. For a typical diameter of an SWNT ($0.5 < d_t < 2$ nm), the Coulomb interaction is sufficiently strong for all carbon atoms along the circumferential direction, so the wave function for the E_{ii} exciton becomes constant around the circumferential direction, which is the reason why we need only one cutting line. When the diameter is sufficiently large compared with the range of the Coulomb interaction (more than 5 nm), the exciton wave function is no longer constant around the circumferential direction (2D exciton), and then we need to use higher-oscillation components from neighboring cutting lines.

Importantly, for the wave function for the E_{ii+1}(E) exciton, which is excited by perpendicularly polarized light, we must consider two cutting lines (i and $i + 1$)

M-SWNTs: metallic single-wall carbon nanotubes

S-SWNTs: semiconducting single-wall carbon nanotubes

[7] Note that E_{ii+1} and E_{i+1i} excitons have E_1 symmetry.

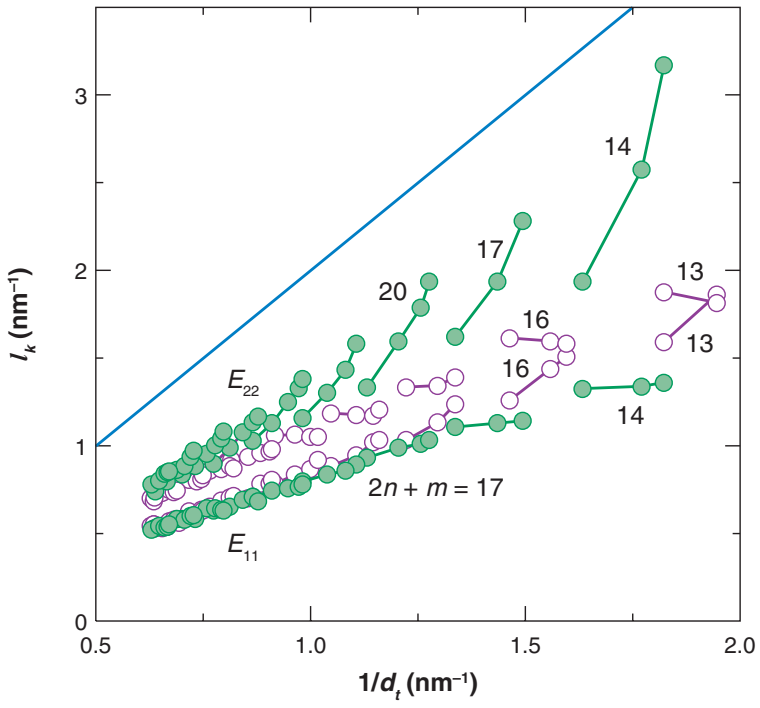

Figure 5

The half-width ℓ_k of the wave functions in one-dimensional k space for the $E_{11}(A_2^0)$ and $E_{22}(A_2^0)$ states. The cutting line spacing $2/d_t$ is shown by the solid line for comparison. Open and filled circles are for SI and SII single-wall carbon nanotubes (SWNTs), respectively, where SI and SII denote the semiconductor tube type in SWNTs. Integers denote the $2n + m$ values for individual SWNTs (17).

(see **Figure 2**) because of the dipole-selection rule. In fact, the calculated exciton has an anisotropy around the circumferential direction in the sense that the electron and hole exist with respect to each other at opposite sides of the nanotube. Uryu and Ando have pointed out that the induced depolarization field (31, 32) cancels the optical field, resulting in a significant upshift of the energy position of E_{ii+1}(E) relative to the $E_{ii}(A)$ exciton (31, 32). This upshift in energy has been observed in PL experiments (28, 33).

3.4. Family Patterns in Exciton Photophysics

Resonance Raman spectroscopy (3) shows that, when the optical transition energies E_{ii} are plotted against tube diameter, they exhibit patterns related to $2n + m =$ constant (see Section 4.5). The family patterns are also observed in 2D PL plots (34). The reason why we get family patterns is that (n, m) SWNTs within the same $2n + m =$ constant family have diameters similar to one another, and E_{ii} values are generally inversely proportional to the diameter. The small change of the E_{ii} values within the

same family is a result of the trigonal warping effect of the electronic dispersion around the K point (29). The trigonal warping effect gives the chirality dependence for both the one-particle energy position at a van Hove singular k point and the corresponding effective mass. The change of the effective mass for the various SWNTs belonging to the same $(2n + n)$ family is important for determining the exciton binding energy and self-energy for each SWNT.

The energy spread in a family becomes large as the diameter decreases and becomes less than 1 nm. In this case, the simple tight-binding calculation, in which we consider only π-electrons, is not sufficient to reproduce the energy positions. To address this problem, the ETB calculation has been developed (5), in which the curvature effect is taken into account by the mixing of the π-orbitals with the σ and $2s$ orbitals of carbon. When we then add the density-functional form of the many-body effect to the ETB results, we can reproduce nicely the experimental results for the dependence of the E_{ii} on diameter and chiral angle (4).

In **Figure 6** we plot the exciton Kataura plot for the $E_{11}^S(A_2^0)$ and $E_{22}^S(A_2^0)$ states for S-SWNTs and the $E_{11}^M(A_2^0)$ states for M-SWNTs. SI and SII SWNTs are defined by mod$(2n + m, 3) = 1$ and mod$(2n + m, 3) = 2$, respectively (29), where mod is a modulus function of an integer. The E_{ii} values are the sum of the ETB one-particle energy, the self-energy Σ, and the exciton binding energy $E_{\rm bd}$. A large family spread appears in **Figure 6**, which is consistent with both calculations (4, 5) and experiments (3, 34).

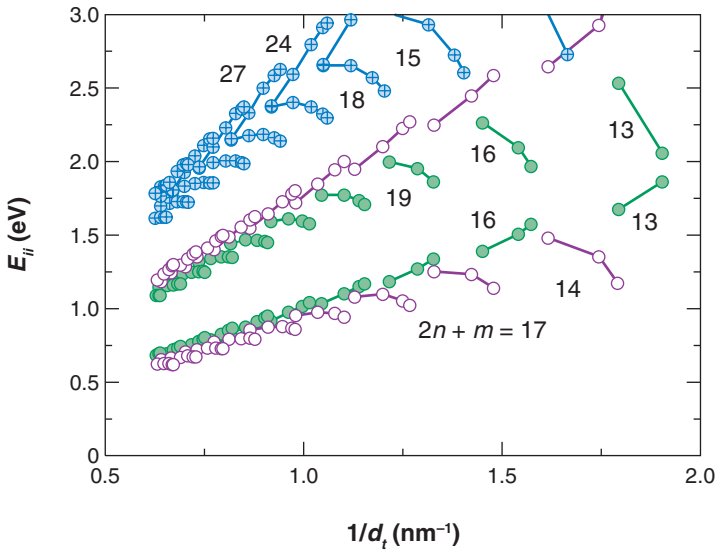

Figure 6

The excitation energy Kataura plot for excitons based on the extended tight-binding (ETB) model for $E_{11}^S(A_2^0)$ and $E_{22}^S(A_2^0)$ for semiconducting single-wall carbon nanotubes (S-SWNTs) and $E_{11}^M(A_2^0)$ for metallic (M-)SWNTs. Open and filled circles are for SI and SII SWNTs, respectively, and crossed circles are for M-SWNTs (17).

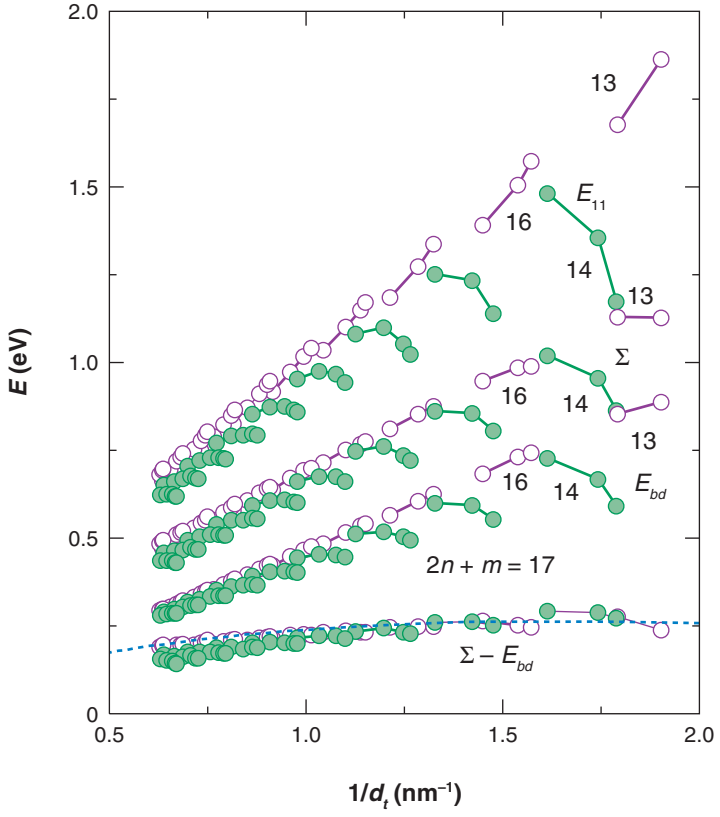

Figure 7

The excitation energy E_{11}^{S}, self-energy Σ, binding energy $E_{\rm bd}$ and energy corrections $\Sigma - E_{\rm bd}$ based on the extended tight-binding (ETB) model for $E_{11}(A_2^0)$ bright exciton states. Open and filled circles are for SI and SII single-wall carbon nanotubes (SWNTs), respectively. The dotted line is calculated by Equation 9 with $p = 1$ (17).

In **Figure 7**, we plot separately each contribution to the ETB excitation energy E_{11}, the self-energy Σ of the quasi-particle, and the exciton binding energy $E_{\rm bd}$. We also plot $\Sigma - E_{\rm bd}$ in the same figure. Although both Σ and $E_{\rm bd}$ tend to increase the family spread, the two values almost cancel each other regarding the family spread, leading to a weak chirality dependence, showing that the net-energy correction ($\Sigma - E_{\rm bd}$) to the single-particle energy depends predominantly on the SWNT diameter. Thus we conclude that the large family spread observed in E_{11} originates from the trigonal warping effect (29) in the single-particle spectra. The logarithmic correction owing to the effect of the Coulomb interaction on the dispersion of 2D graphite is not canceled by the exciton binding energy and leads to a logarithmic energy correction $E^{\log}$ given by (4, 19)

$$E^{\log} = 0.55(2p/3d_t)\log[3/(2p/3d_t)]. \qquad (9)$$

In **Figure 7**, we plot $E^{\log}$ with $p = 1$ as a dashed line, thus showing that our energy correction $\Sigma - E_{\rm bd}$ follows this logarithmic behavior well. This good agreement for $\Sigma - E_{\rm bd}$ explains why the previous treatment of the ETB model (5, 55) works so well and how it includes many-body effects.

4. EXPERIMENTAL EVIDENCE FOR EXCITONS IN CARBON NANOTUBES

As discussed in Section 1, the so-called ratio problem first brought into sharp focus experimentally the importance of many-body effects in SWNTs (1, 19). Section 4.1 presents the physics behind this problem, representing the first evidence in which electron-electron and electron-hole interactions explained an experimental observation in SWNTs. Subsequently, reported experiments gave definitive evidence for the need for excitonic effects to explain the photophysics observations. The two-photon absorption experiments gave experimental evidence for the presence of excited exciton states (Section 4.2). The lineshape analysis of the PL side bands further proved the existence of exciton-phonon complexes (Section 4.3). The exciton binding energy (E_b) was extracted from different experiments, showing a diameter dependence as predicted by theory (Section 4.4). Although the excitonic picture seems clear for the first two optical levels in S-SWNTs, understanding of the many-body effects for the higher-lying levels (E^S_{33} and E^S_{44}) and for M-SWNTs still needs further development (Section 4.5).

4.1. Exciton Energies and the Ratio Problem

In **Figures 8*a*,*b***, we show the calculated ratio E^S_{22}/E^S_{11} as a function of $1/d_t$ for bright excitons with and without the Coulomb interaction, respectively. As seen in **Figure 8**, the E^S_{22}/E^S_{11} ratios for individual tubes depend on chiral angle and tube type (**Figure 7**). If we extrapolate the averaged value of E^S_{22}/E^S_{11} for each family to $1/d_t \rightarrow 0$ for very large tube diameter,[8] we can see a clear difference between (*a*) 1.8 and (*b*) 2. If we do not consider the Coulomb interaction, the extrapolated value should be 2 (**Figure 8*a***). However, the experimental results (34) always show a smaller value around 1.8. This difference is called the ratio problem (19). The ratio problem was the experimental evidence that led to a strong consideration of many-body effects (7, 8, 11, 12, 17, 19, 28, 35).

In the one-particle picture, the E_{ii} values are expected to exhibit a simple diameter dependence when plotted as a function of p/d_t, where $p = 1, 2, 3, 4,$ and 5 for E^S_{11}, E^S_{22}, E^M_{11}, E^S_{33}, and E^S_{44}, respectively (24, 29). We can understand this behavior by relating the electronic structure of SWNTs to that of 2D graphite (or graphene), subject to the quantization of the wave vector $|\mathbf{K}_1| = 2/d_t$ along the tube circumference. The linear energy-momentum relation for electrons in graphene is unusual and

[8] If we take the limit of $d_t \rightarrow \infty$, the exciton becomes two dimensional. In this case we may neglect the exciton binding energy compared with the self-energy correction.

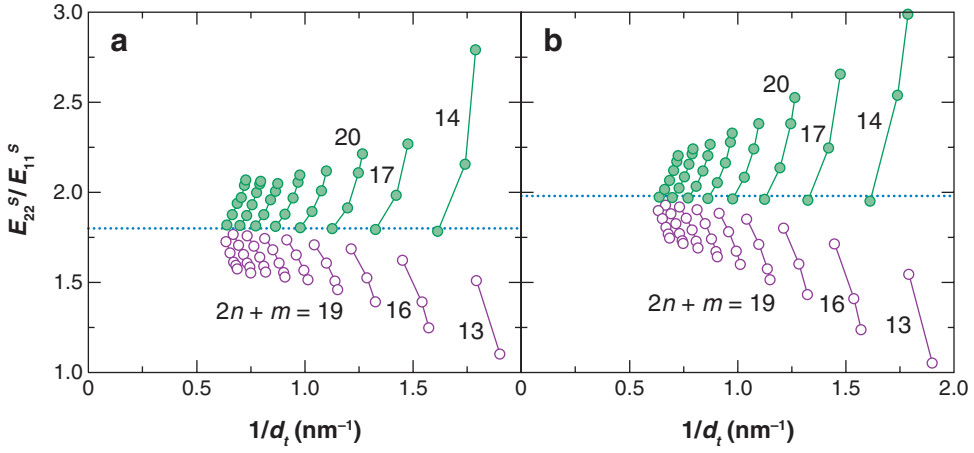

Figure 8

The excitation energy ratio E_{22}^S/E_{11}^S for A_2^0 states based on the extended tight binding (ETB) model for semiconducting single-wall carbon nanotubes (S-SWNTs) with 0.5 nm $< d_t <$ 1.6 nm. Open and filled circles are for SI and SII SWNTs. Panels *a* and *b* are the results with and without considering the Coulomb interaction, respectively. Dotted lines indicate the values for the average E_{22}^S/E_{11}^S ratio (17).

is given by $E = \pm\hbar v k$ (where v is the electron velocity). Quantization of the wave vector restricts the allowed wave vectors measured from the K point to $k = 2p/3d_t$. As a first approximation, the optical transition energies in carbon nanotubes are given by (29)

$$E_{ii} = 4p\hbar v/3d_t. \tag{10}$$

Thus we expect the ratio E_{22}^S/E_{11}^S ($p = 2$ and 1 for E_{22}^S and E_{11}^S, respectively) to be equal to 2 in the limit of $d_t \to \infty$. For a finite diameter, we expect the E_{ii} values to exhibit a dependence on chiral angle θ (ranging from 0 to 30°) because of the trigonal warping effect (29). The trigonal warping effect is zero for armchair tubes ($\theta = 30°$), is a maximum for zigzag tubes ($\theta = 0$), and is given approximately by $\beta_p \cos 3\theta/d_t^2$ for chiral tubes.

Although the E_{22}^S/E_{11}^S ratio problem was observed by optical-absorption experiments (36), it was not until it was reported in the PL spectra for isolated SWNTs in 2002 (34, 37) that the scientific community started systematic work on this problem. In the PL experiment (34), the SWNT sample was excited at E_{22}^S, and the emission from the E_{11}^S level was recorded. This ratio problem was explained by considering many-body effects (19). The electron-electron repulsion causes a blue shift and the electron-hole excitonic attraction causes a red shift in the electronic transition energies (7, 19). The net energy change is a blue shift for both the E_{11}^S and E_{22}^S levels, which makes the $d_t \to \infty$ limit of the E_{22}^S/E_{11}^S ratio decrease from 2 to 1.8.

4.2. Measurement of Excited Exciton States

Further experimental evidence for the excitonic nature of the optical transition in carbon nanotubes came from measurements of excited excitonic states (37a), with the most striking experimental result from nonlinear two-photon absorption experiments by using very high-power laser pulses (9, 10). In this experiment, SWNTs are excited in a two-photon absorption process at energies (E_{laser}) somewhat above half the first optical transition energy for S-SWNTs ($E_{laser} \geq E_{11}^S/2$), and subsequent light emission is observed around E_{11}^S. If the optically induced transitions E_{11}^S were related to free electron-hole pairs making band-to-band transitions, then the absorption of the two photons would occur at exactly $\left(E_{laser} = E_{11}^S/2\right)$ (see **Figure 9*a***). However, if the E_{11}^S optical level were related to the creation of an exciton, then the energy for the absorption of two photons would be observed at an excited exciton state with an energy higher than E_{11}^S. Such a difference in energy between the absorption and emission processes was observed experimentally (see **Figure 9*a***), thus giving strong support for the exciton model.

PLE: photoluminescence excitation

However, group theory (23) does not predict the selection rules cited in reports on these two recent photon experiments (9, 10), and the explanation of the results obtained in two-photon excitation experiments does not rely on symmetry selection rules (23). The explanation for the observed excitonic behavior rather comes from the optical-absorption oscillator strength (10), which in the case of two-photon absorption, is very small for the lowest-energy bright exciton state (see calculated results in **Figure 9*b***). For instance, we can understand the bright exciton expected for odd ν states in chiral tubes as a product between an odd Bloch function and an odd envelope function. Therefore, we nevertheless expect a very low oscillation strength for these A_1 symmetry excitons, although being formally bright, because an odd envelope function should give a very low probability of finding an electron and a hole at the same spatial position, available for recombination.

Theory was used to predict the results obtained by the two-photon absorption experiment. The calculated values for the exciton binding energy (18) were found to account well for the experimental observations once the environmental conditions relevant to each of the different experiments were taken into account (17).

4.3. The Exciton-Phonon Side Bands

Another strong indication that the optical properties of carbon nanotubes are excitonic rather than having one-electron band-like wave functions comes from the experimental observation of exciton-phonon complexes (20, 37–39), demonstrating both the existence of excitons and the central role played by phonons in describing the excitation and recombination mechanisms in carbon nanotubes.

Figure 10*a* shows a 2D photoluminescence excitation (PLE) plot obtained by measuring PLE spectra with 51 excitation energies, from 1.20 eV through 1.75 eV (20). In the PLE map, the emission energies are along the horizontal axis, and the excitation energies are along the vertical axis. For the excitation range used in this work, several resonances are observed depending on the excitation energy, although

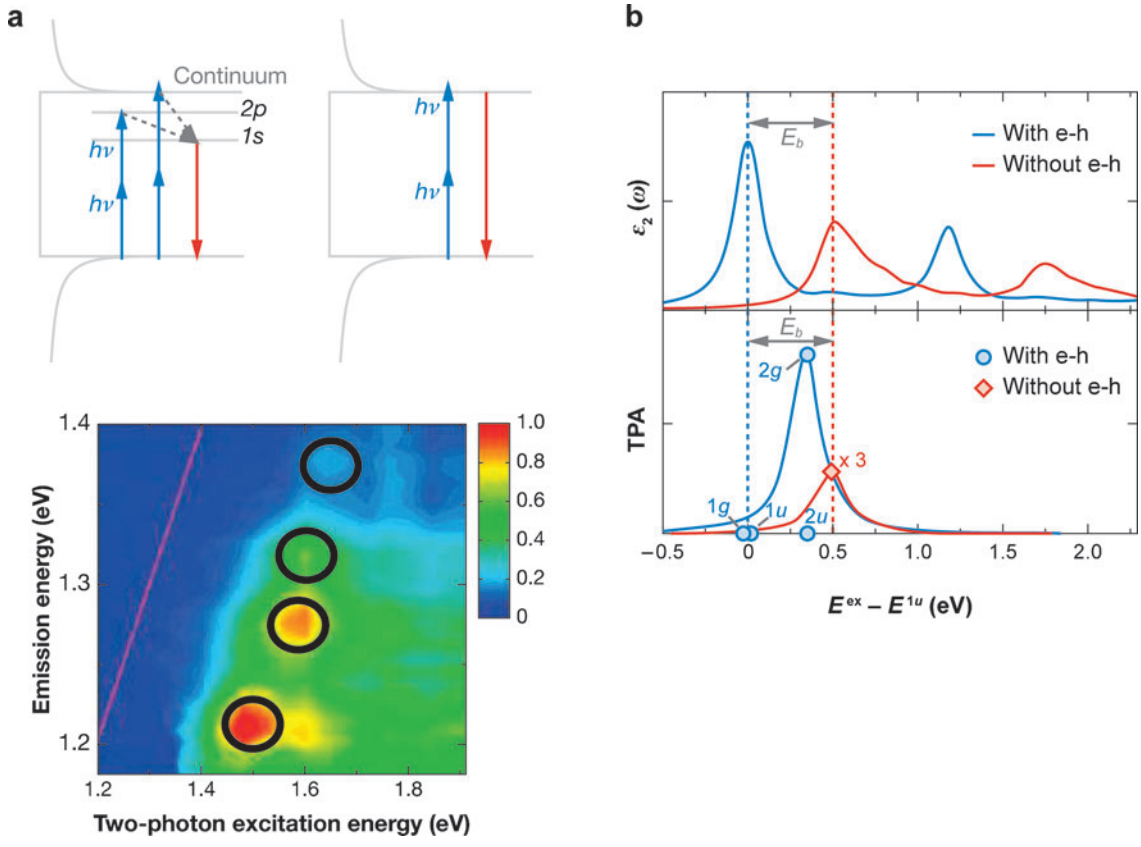

Figure 9

(*a*) A schematic representation (*top*) of the single-wall carbon nanotube (SWNT) density of states, showing the absorption of two photons and the emission of one photon with (*left*) and without (*right*) excitons. (*Bottom*) A contour plot of the two-photon excitation spectra of SWNTs (9). The line is plotted for $E_{em} = E_{TPA}$, whereas the black circles mark the higher two-photon absorption energy E_{TPA} and the lower-lying one-photon emission energy E_{em} for different (n, m) tubes. Emission always occurs at $E_{em} = E_{11}^{S} < E_{TPA}$ (9). (*b*) Ab initio calculated one-photon [$\varepsilon_2(\omega)$, *top*] and two-photon absorption profiles (TPA, *bottom*) for the (6, 4) SWNT. Blue lines are with electron-hole interactions, whereas red lines are without. Higher-energy states with negligible amplitudes are omitted for clarity (10). Here the experimentally measured exciton binding energy E_b is defined as the energy difference between the band edge without electron-hole interaction and the lowest-energy bright excitonic state labeled 1 *g*.

the recombination process is observed at the same band edge energy (labeled by E_{11}^{1s} in **Figure 10*a***). The resonances for which the excitation and emission energies are the same (E_{11}^{S}) appear as a 45° line at the lower right corner of the PLE map in **Figure 10*b***. The absorption profile is obtained by performing a vertical cut in the PLE map of **Figure 10*a*** at energies that correspond to the emission of a given nanotube. **Figure 10*b*** shows the plot of such a profile for the (8, 3) SWNT.

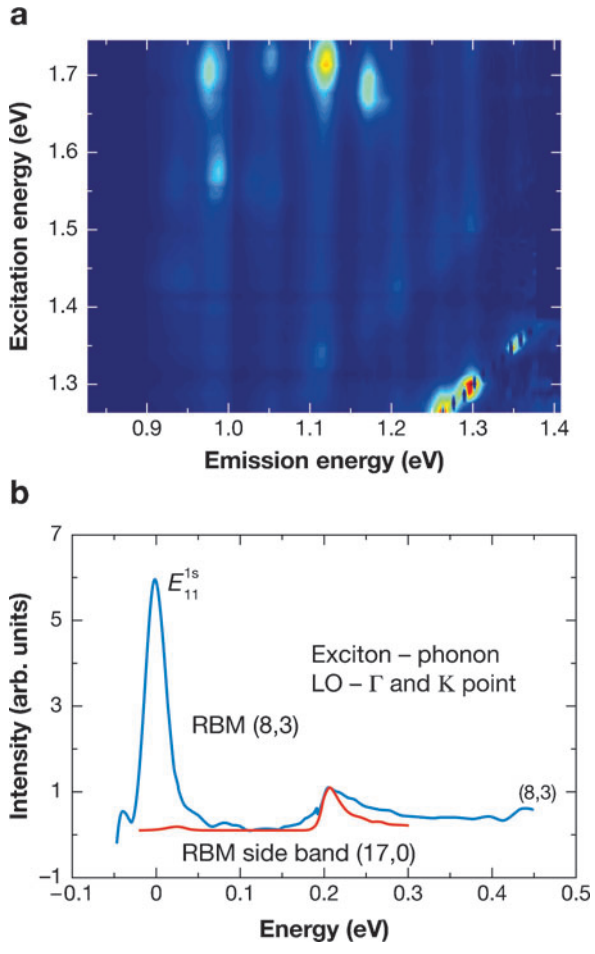

Figure 10

(*a*) A photoluminescence excitation (PLE) plot of the emission obtained using 51 excitation energies between 1.25 and 1.75 eV. Colors changing from dark blue to red indicate an increase in emission intensity. Each vertical streak in the map represents an emission peak from a given single-wall carbon nanotube (SWNT), and a high-intensity spot in the map is associated with a resonance in the PLE spectra. (*b*) PLE spectrum taken at 1.30 eV showing the bright exciton close to the band edge, and the phonon side band approximately 200 meV higher in energy with an (8, 3) SWNT (20).

Well-resolved resonances, approximately 200 meV above each $E_{11}(A_2)$ feature, can also be observed in the PLE map and could be related to a resonance Raman process in which the incoming photon has an energy $\hbar\omega_{in} = \hbar\omega_{out} + \hbar\omega_G$, where ω_G is the frequency of the *G*-band phonon. This possibility is ruled out owing to both the asymmetric lineshapes of the PLE profile in **Figure 10*b*** and the small upshift of the frequency of the phonon side peak relative to $\hbar\omega_G$.

Furthermore, a *G*-band Raman process obtained by taking a horizontal cut in the PLE map would be expected to have a much narrower Lorentzian lineshape, and its resonance profile would not have a broad lineshape elongated toward the high-energy side as observed in the experimental trace in **Figure 10*b***. Perebeinos et al. (14) therefore proposed that the observed side band should be assigned to a resonance identified with the absorption of light to a bound exciton-phonon state. The main contribution to the exciton-phonon bound state observed in **Figure 10*b*** is attributed to the longitudinal optical phonon at the **K** and Γ points of the graphene BZ (14). In such a situation, a significant fraction of the spectral weight should be transferred from the exciton peak to the exciton-phonon complex, and this transferred spectral weight is predicted to have a diameter dependence. A clear trend is observed experimentally (20), showing that larger diameter tubes have a lower spectral weight transfer than smaller diameter tubes, as predicted theoretically, although some (n, m) chirality dependence is also observed (14).

4.4. Exciton Binding Energy

A key issue in exciton physics generally is the determination of the magnitude of the exciton binding energy for the various E_{ii} excitonic states. This has been a difficult task in carbon nanotubes because the onset of the continuum for a given exciton (such as the E_{11}^S or E_{22}^S excitons) has not directly been observed on an experimental basis.[9]

Much of our present knowledge of the exciton binding energy has been extracted from nonlinear two-photon absorption experiments that have been carried out using 130-fs (9) and 150-fs (10) laser pulses for creating the two-photon excited state. In those experiments, researchers measured the energy difference between the ground state and the lowest-energy bright exciton of the E_{11}^S levels, and used the results to calibrate the dielectric constant of the environment based on a first-principles theory (10). Next, from theory and a lineshape analysis of the experimental data, they determined the exciton binding energies E_b for different (n, m) SWNTs. The authors get results consistent with each other, roughly given by $E_b = 0.3/d_t$ in electron volts. This result is in agreement with theory using a dielectric constant of $\kappa = 2.22$ (17). Here E_b denotes the experimentally determined binding energy in which environmental effects must be considered in contrast to the theoretical binding energy E_{bd} discussed in Section 3 in which no environmental effects enter.

Two-color pump-probe studies using 50-fs pulses provided a direct measurement of the binding energy of the E_{11} exciton by initial excitation at a transition energy of either E_{22}^S (660 nm, 1.88 eV) or E_{11}^S (953 nm, 1.30 eV), corresponding to the E_{11}^S and E_{22}^S bright exciton energies for an (8, 3) nanotube (40). A high-probability decay route for the exciton at E_{22}^S is the nonradiative decay of the E_{22}^S exciton states to E_{11}^S, a decay process commonly reported in PL experiments (1, 34). Therefore, under

[9]The onset of the continuum may be defined theoretically as the one-particle energy plus the self-energy correction for a delocalized electron (or hole). Because the self-energy correction for an exciton should be larger than that for a delocalized wave function, the direct comparison between theory and experiment should be treated in more detail in the future.

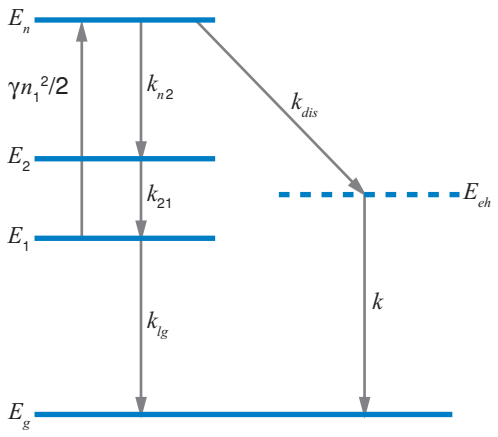

Figure 11

Schematic description of the electronic structure of the (8, 3) single-wall carbon nanotube (SWNT) and the excitonic relaxation pathways obtained from fast-optics experiments (40). Here E_g and E_i represent the ground state and the i-th excited states (E_{ii} in the notation of the present review), respectively, whereas E_{eh} denotes the band edge for the electron-hole continuum. The downward arrows depict the relaxation pathways with corresponding relaxation rates as labeled schematically, and the upward arrow denotes the process of populating a higher exciton state as the result of exciton-exciton annihilation in an Auger process.

high-power pulse excitation, a high density of E_{11}^S excitonic states is achieved in the fast-optics experiment (40), independent of whether the initial excitation is at E_{22}^S or E_{11}^S.

Fast optics: refers to experiments done in the time domain when a light pulse of less than 200 fs is used

The decay of these E_{11}^S excitonic states involves predominantly the bimolecular exciton-exciton annihilation of two E_{11}^S excitons through an Auger process by which higher energy states, such as E_n, are accessed (see **Figure 11**). These higher energy states soon decay nonradiatively either to the E_{11} bright exciton state denoted by E_1, or alternatively to E_{eh}, in **Figure 11**, which is identified with the lowest continuum state for the E_{11} transition. The crucial point about this experiment is the finding that excitations at both E_{11} and E_{22} lead, through the processes discussed above, to a well-resolved feature in the induced transient absorption spectrum at the E_{eh} energy measured experimentally to be 730 nm (1.70 eV). The energy difference between E_{eh} and E_{11} is thus measured directly to be 0.40 eV, and this energy is identified with the binding energy of the E_{11} exciton for the (8, 3) tube. This result for the (8, 3) SWNT is in good agreement with experimental measurements on the (8, 3) SWNT using the two-photon absorption technique of 0.42 eV by Wang et al. (9) and Dukovic et al. (41), and of 0.38 eV by Maultzsch et al. (10).

Finally, values for the exciton binding energy have been reported for E_{22}^S through combined resonance Raman and electrochemistry doping experiments for the two (n, m) SWNTs (42). By applying a voltage, the authors change the Fermi level, and the RBM signal is observed to disappear when filling the conduction band, or removing electrons from the valence band. By comparing the excitonic energy with the

energy necessary to fill/empty the band levels, the authors extract the binding energy. Importantly, theory predicts different binding energies for the bright E_{22} exciton as compared with the E_{11} bright exciton owing to changes in the effective mass and screening effects for these bright excitons. Few measurements are so far available for the binding energy for E_{22}^S excitons, and theoretical estimates for the (7, 5) and (10, 3) tubes yield E_b values of 0.55 eV using $\kappa = 2.56$ for the dielectric constant (18).

4.5. The Diameter-Dependent Scaling Law for E_{ii}^S and Metallic Carbon Nanotubes

Resonance Raman spectroscopy, performed with a quasi-continuous set of excitation laser lines (E_{laser}), was used to build a 2D plot (Raman intensity as a function of E_{laser} and ω_{RBM}), as shown in **Figure 12** (3, 43–45). In this figure, a Raman peak appears at a given ω_{RBM} whenever the laser energy is equal to the optical transition energy (i.e., when the resonance condition is best established for a given carbon nanotube in the sample) (3). From each peak in the experimental plot (**Figure 12**), we can extract the (E_{ii}, d_t) for each resonant SWNT. Using the relation $d_t = a_{\text{C–C}}\sqrt{3(n^2 + mn + m^2)}/\pi$, where $a_{\text{C–C}} = 0.142$ nm is the carbon-carbon distance (24), we can obtain ω_{RBM} from the relation between ω_{RBM} and the tube diameter, $\omega_{\text{RBM}} = A/d_t + B$, with $A = 218$ cm^{-1} nm and $B = 16$ cm^{-1} (43).

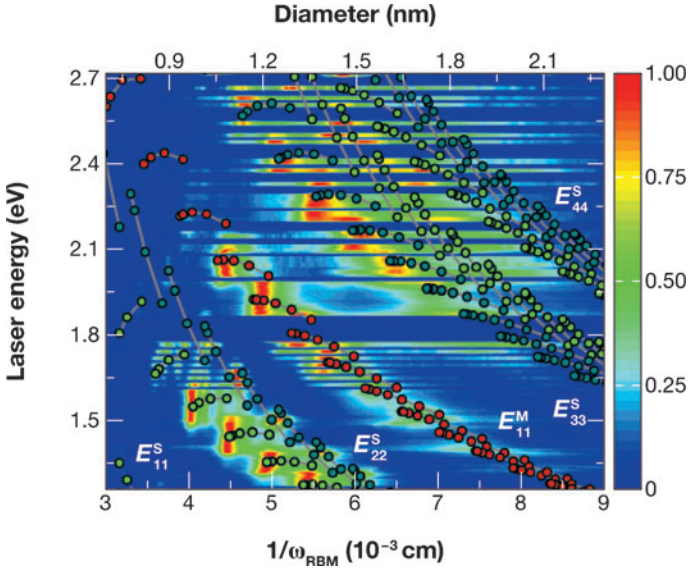

Figure 12

Two-dimensional color map showing the single-walled carbon nanotube (SWNT) spectral evolution as a function of excitation laser energy. Superposed are the 378 optical transition energies (*dots*) of all SWNTs in the experimental range, plotted as a function of diameter d_t. Gray lines are guides for the family patterns formed by SWNTs with $2n + m =$ constant (43).

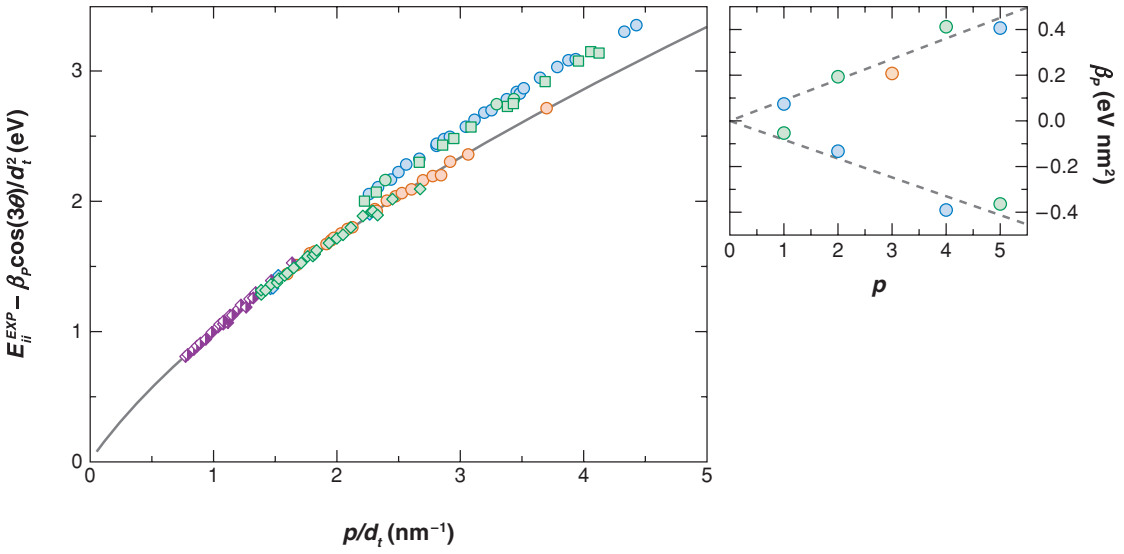

Figure 13

Experimental optical transition energies as a function of p/d_t, after correcting for the chiral angle dependence ($E_{ii}^{EXP} - \beta_p \cos 3\theta/d_t^2$). The chirality-dependence-corrected points for E_{11}^S (*purple and white diamonds* from Reference 34), E_{22}^S (*green squares*), and E_{11}^M (*orange circles*) energies (43) are fitted with Equations 9 and 10. (*Side graph*) The β_p constants obtained experimentally for $p = 1$ to 5, and these constants can be fit by $\beta_p^+ = p(0.087 \pm 0.008)$ eV nm^2 and $\beta_p^- = p(-0.085 \pm 0.007)$ eV-nm^2 (*dashed lines*).

The results thus obtained for ω_{RBM} and E_{ii} are in good agreement with most prior work, including resonance Raman spectroscopy (3, 44, 45) and PL measurements (34). Rayleigh scattering has also been used to measure E_{33}^S and E_{44}^S, E_{11}^M, and E_{22}^M, and the results are also in good agreement with the values depicted in **Figure 12** (46).

Figure 13 shows a plot of the E_{11}^S [from PL experiments (34)], and E_{22}^S, E_{11}^M, E_{33}^S, E_{44}^S [mostly from resonance Raman measurements (43)] as a function of p/d_t, obtained by subtracting $\beta_p \cos 3\theta/d_t^2$ from the experimentally obtained E_{ii} values, to correct for their chiral angle dependence. Such a chirality correction is expected to collapse all the E_{ii} values onto a single (p/d_t)-dependent curve (4, 47). The points do not scale linearly as p/d_t. The nonlinear scaling is a result of many-body effects, which are also responsible for the E_{22}^S/E_{11}^S ratio problem discussed in Section 4.1 (19, 34, 47).

There are two interesting and intriguing conclusions from **Figure 13**. First, the E_{33}^S and E_{44}^S transitions do not follow the same scaling law as the E_{11}^S and E_{22}^S transitions, implying possible differences in the many-body effects for the higher- and lower-lying transitions. These differences do not seem to be captured by the solid-state physics model (see Section 3 and Reference 7), in which the exciton binding energy increases for the third level. These differences can, however, be explained by quantum chemistry–based calculations (43) that show rather delocalized or even unbound excitonic states for the E_{33} level. Another interesting result comes from the

electronic transition energies from metallic tubes. Metallic materials are expected to exhibit different many-body effects when compared with semiconducting materials because of the screening by free electrons in metals. Usually metallic systems do not exhibit real excitons, but rather excitonic resonances, because they can always decay into the continuum of states. The observation of excitons in metallic carbon nanotubes has been explained as an interesting symmetry-related effect (7). The possibility for a symmetry-based explanation for the observation of the two different scaling laws observed in **Figure 13** (43) has to be addressed theoretically and experimentally. The single scaling law for the E_{11}^S, E_{22}^S, and E_{11}^M nanotube excitonic levels (4, 43) is an interesting phenomena of 1D systems, probably owing to the near cancellation of the repulsive electron-electron by the attractive electron-hole interactions (7, 19).

5. OUTLOOK

In summary, we review the excitonic properties of carbon nanotubes. The large binding energy of an exciton in SWNTs allows the observation of many exotic excitonic phenomena at room temperature. The unique electronic structure of carbon nanotubes gives rise to four different symmetries for excitons in SWNTs: A_1, A_2, E, and E^*, in which only the A_2 symmetry exciton with $S = 0$ is a bright (light-emitting) exciton. The exciton binding energy and the self-energy correction term to the one-particle energy are calculated by the Bethe-Salpeter equation. The calculated results show that (*a*) the self-energy is larger than the exciton binding energy, (*b*) the exciton wave function is localized along only one cutting line in k space, (*c*) a dark exciton is the lowest energy state below the lowest bright exciton, and (*d*) the family-related spread in the electron-hole attractive energy and electron-electron self-energy almost cancel each other. Thus the family behavior is understood on the basis of one-electron-based models. The excited-exciton-state wave functions have odd symmetry with regard to the direction of the nanotube axis, which we can observe by a two-photon absorption experiment. The exciton binding energy has been recently measured by fast-optics methods. The existence of the lowest-energy dark exciton and its physical properties are now being investigated by the temperature and magnetic-field dependence of the observed PL features (48–53).

Although there have been many investigations of the exciton states in SWNTs, there are still many issues that require further experimental and theoretical investigation. The exciton-phonon interaction still needs to be investigated using exciton wave functions to determine the relaxation rates and the spectral intensities for the various phonons of importance. Exciton formation and dissociation will likely be observed by several other experimental techniques, and theoretical understanding of these experiments will then be necessary. The dynamics and decay of the various excitonic states and the transformations between dark and bright excitons remain key issues for understanding the low PL quantum efficiency of the excitonic states observed in real SWNT systems, and here careful experiments on freely suspended tubes (54) will show the role of environmental effects in quenching the PL emission for tubes interacting with substrates. Such studies are likely to launch systematic

studies of environmental effects of the substrates, wrapping agents, and solvation on the various photophysical techniques in current use. The use of perturbation techniques to transform dark to bright excitons will enhance the exciton intensity significantly.

More generally, the use of symmetry-breaking perturbations (such as uniaxial stress, doping, and magnetic fields) is an important research direction for gaining a better understanding of nanotube optics. Comparison between scanning tunneling spectroscopy and PL emission will give valuable information regarding the difference between the one-particle picture and the pseudoparticle models. The study of excitons in metallic nanotubes and in higher E_{ii} states remains an interesting and open research area, both in understanding environmental effects and in comparison with the excitonic behavior of semiconducting nanotubes or of lower-energy E_{ii} states. 1D diffusive motion of excitons and exciton-polariton physics are likely to become active topics of future study. Furthermore, we expect 1D exciton studies to become more important in the future, especially as more 1D systems in the form of nanowires and nanotubes are developed. Carbon nanotube photophysics has already profited significantly from the knowledge about excitonic effects coming from π-conjugated polymers, and the merging of chemistry and physics would also be expected to affect the development of other 1D systems. Thus we can expect the basic science of excitons in nanotubes to attract increasing interest as an important prototype system for studying 1D excitons in the future.

SUMMARY POINTS

1. Strong exciton effects can be observed at room temperature because of the 1D nature of SWNTs.
2. The Bethe-Salpeter equation based on the ETB model provides a good description for the excitonic behavior of SWNTs.
3. $(2n + m)$ family behavior plays a major role in the photophysics of small-diameter SWNTs.
4. The low efficiency of the PL process (down by approximately three orders of magnitude) is a result of multiple dark exciton states below the lowest lying bright exciton state.
5. Optical transition energies for bright excitons are quantitatively probed by resonance Raman scattering and PL.
6. Two-photon absorption and phonon side band experiments give strong evidence for excitons.
7. Although current theoretical models account for the observed excitonic behavior for E_{11} and E_{22} transitions for S-SWNTs, many unexplained effects are observed for E_{33} and E_{44} transitions.
8. Little is presently known about dark singlet and triplet excitonic states in SWNTs.

ACKNOWLEDGMENTS

M.S.D. and G.D. gratefully acknowledge support from NSF grant DMR04-05538. R.S. acknowledges support from NEXT grant (no. 16076201). A.J. acknowledges financial support from FAPEMIG and CNPq, Brazil. The authors also acknowledge stimulating discussions with Ge. G. Samsonidze, E. Barros, Dr. J. Jiang, Prof. M.A. Pimenta, and Prof. R.B. Capaz.

LITERATURE CITED

1. O'Connell MJ, Bachilo SM, Huffman XB, Moore VC, Strano MS, et al. 2002. Band gap fluorescence from individual single walled carbon nanotubes. *Science* 297:593–96
2. Dresselhaus MS, Dresselhaus G, Saito R, Jorio A. 2005. Raman spectroscopy of carbon nanotubes. *Phys. Rep*. 409:47–99
3. **Fantini C, Jorio A, Souza M, Strano MS, Dresselhaus MS, Pimenta MA. 2004. Optical transition energies for carbon nanotubes from resonant Raman spectroscopy: environment and temperature effects. *Phys. Rev. Lett*. 93:147406**
4. Jorio A, Fantini C, Pimenta MA, Capaz RB, Samsonidze GG, et al. 2005. Resonance Raman spectroscopy (n, m) dependent effects in small diameter single-wall carbon nanotubes. *Phys. Rev. B* 71:075401
5. **Samsonidze GG, Saito R, Kobayashi N, Grüneis A, Jiang J, et al. 2004. Family behavior of the optical transition energies in single-wall carbon nanotubes of smaller diameters. *Appl. Phys. Lett*. 85:5703–5**
6. Ando T. 1997. Excitons in carbon nanotubes. *J. Phys. Soc. Jpn*. 66:1066–73
7. **Spataru CD, Ismail-Beigi S, Benedict LX, Louie SG. 2004. Excitonic effects and optical spectra of single-walled carbon nanotubes. *Phys. Rev. Lett*. 92:077402**
8. Spataru CD, Ismail-Beigi S, Benedict LX, Louie SG. 2004. Quasiparticle energies, excitonic effects and optical spectra of small diameter single-walled carbon nanotubes. *Appl. Phys. A* 78:1129–36
9. **Wang F, Dukovic G, Brus LE, Heinz TF. 2005. The optical resonances in carbon nanotubes arise from excitons. *Science* 308:838–41**
10. **Maultzsch J, Pomraenke R, Reich S, Chang E, Prezzi D, et al. 2005. Exciton binding energies in carbon nanotubes from two-photon photoluminescence. *Phys. Rev. B* 72:241402**
11. Spataru CD, Ismail-Beigi S, Capaz RB, Louie SG. 2005. Theory and ab initio calculation of radiative lifetime of excitons in semiconducting carbon nanotubes. *Phys. Rev. Lett*. 95:247402
12. Chang E, Bussi G, Ruini A, Molinari E. 2004. Excitons in carbon nanotubes: an ab initio symmetry-based approach. *Phys. Rev. Lett*. 92:113410
13. **Perebeinos V, Tersoff J, Avouris P. 2004. Scaling of excitons in carbon nanotubes. *Phys. Rev. Lett*. 92:257402**
14. Perebeinos V, Tersoff J, Avouris P. 2005. Effect of exciton-phonon coupling in the calculated optical absorption of carbon nanotubes. *Phys. Rev. Lett*. 94:027402

3. Presents resonance Raman scattering measurements of the excitonic E_{ii} values for SWNTS and their consistency with PL measurements.

5. Demonstrates an exposition of the ETB model, which has been widely used for the analysis of Raman and PL measurements.

7. Presents ab initio calculations of excitonic effects and optical spectra of SWNTs.

9 & 10. Describes two-photon absorption experiments giving strong support for excitonic effects in SWNTs.

13. Presents the calculation of the scaling relation of excitions in SWNTs.

15. Pedersen TG. 2003. Variational approach to excitons in carbon nanotubes. *Phys. Rev. B* 67:073401
16. Zhao H, Mazumdar S. 2005. Excitons in semiconducting single-walled carbon nanotubes. *Synth. Met.* 155:250–53
17. Jiang J, Saito R, Samsonidze GG, Jorio A, Chou SG, et al. 2006. Chirality dependence of the exciton effects in single-wall carbon nanotubes. *Phys. Rev. B*. In press
18. Capaz RB, Spataru CD, Ismail-Beigi S, Louie SG. 2006. Diameter and chirality dependence of exciton properties in carbon nanotubes. *Phys. Rev. B.* 74:121401
19. Kane CL, Mele EJ. 2003. Ratio problem in single nanotube fluorescence spectroscopy. *Phys. Rev. Lett.* 90:207401
20. Plentz F, Ribeiro HB, Jorio A, Strano MS, Pimenta MA. 2005. Direct experimental evidence of exciton-phonon bound states in single-wall carbon nanotubes. *Phys. Rev. Lett.* 95:247401
21. Rohlfing M, Louie SG. 2000. Electron-hole excitations and optical spectra from first principles. *Phys. Rev. B* 62:4927–44
22. Barros EB, Jorio A, Samsonidze GG, Capaz RB, Filho AG, et al. 2006. Review on the symmetry related properties of carbon nanotubes. *Phys. Rep.* 431:261–302
23. Barros EB, Capaz RB, Jorio A, Samsonidze GG, Filho AG, et al. 2006. Selection rules for one- and two-photon absorption by excitons in carbon nanotubes. *Phys. Rev. B* 73:241406
24. Saito R, Dresselhaus G, Dresselhaus MS. 1998. *Physical Properties of Carbon Nanotubes*. London: Imperial College Press
25. Samsonidze GG, Saito R, Jorio A, Pimenta MA, Souza Filho AG, et al. 2003. The concept of cutting lines in carbon nanotube science. *J. Nanosci. Nanotechnol.* 3:431–58
26. Saito R, Sato K, Oyama Y, Jiang J, Samsonidze GG, et al. 2005. Cutting lines near the Fermi energy of single-wall carbon nanotubes. *Phys. Rev. B* 71:153413
27. Knox RS. 1963. *Theory of Excitons. Solid State Physics Suppl. 5*, ed. F Seitz, D Turnbull, H Ehrenreich. New York: Academic
28. Ando T. 2005. Theory of electronic states and transport in carbon nanotubes. *J. Phys. Soc. Jpn*. 74:777–817
29. Saito R, Dresselhaus G, Dresselhaus MS. 2000. Trigonal warping effect of carbon nanotubes. *Phys. Rev. B* 61:2981–90
30. Qiu X, Freitag M, Perebeinos V, Avouris P. 2005. Photoconductivity spectra of single-carbon nanotubes: implications on the nature of their excited states. *Nano Lett*. 5:749–52
31. Ajiki H, Ando T. 1994. Physics of carbon nanotubes. *Phys. B* 201:349–52
32. Uryu S, Ando T. 2006. Prominent exciton effects on absorption of perpendicularly polarized light in carbon nanotubes. *J. Phys. Soc. Jpn*. 75:024707
33. Maruyama S, Miyauchi Y. 2005. Phonon sideband in optical spectra of C^{13} carbon nanotubes. *Proc. XVIII Int. Winter School Electron. Prop. Novel Mater*. 786:100–5

17. Develops the chirality dependence of exciton effects in SWNTs based on the Bethe-Salpeter equation.

19. Presents the ratio problem about $E_{22}^S/E_{11}^S \neq 2$ observed in single nanotube fluorescence spectroscopy.

20. Describes an observation of exciton-phonon side bands by PLE spectroscopy.

22. Describes symmetry aspects of carbon nanotubes and their excitonic behavior.

24. Presents an introductory text for carbon nanotubes.

34. Bachilo SM, Strano MS, Kittrell C, Hauge RH, Smalley RE, Weisman RB. 2002. Structure-assigned optical spectra of single walled carbon nanotubes. *Science* 298:2361–66
35. Ando T. 2004. Excitons in carbon nanotubes revisited: dependence on diameter, Aharonov-Bohm flux, and strain. *J. Phys. Soc. Jpn*. 73:3351–53
36. Ichida M, Mizuno S, Saito Y, Kataura H, Achiba Y, Nakamura A. 2002. Coulomb effects on the fundamental optical transition in semiconducting single-walled carbon nanotubes: divergent behavior in the small-diameter limit. *Phys. Rev. B* 65:241407
37. Miyauchi Y, Maruyama S. 2006. Identification of an excitonic phonon sideband by photoluminescence spectroscopy of single-walled carbon-13 nanotubes. *Phys. Rev. B* 94:035415
37a. Korovyanko OJ, Sheng CX, Vardeny ZV, Dalton AB, Baughman RH. 2004. Ultrafast spectroscopy of excitons in single-walled carbon nanotubes. *Phys. Rev. Lett*. 92:017403
38. Chou SG, Plentz Filho F, Jiang J, Saito R, Nezich D, et al. 2005. Phonon-assisted excitonic recombination channels observed in DNA-wrapped carbon nanotubes using photoluminescence spectroscopy. *Phys. Rev. Lett.* 94:127402
39. Htoon H, O'Connell MJ, Doorn SK, Klimov VI. 2005. Single carbon nanotubes probed by photoluminescence excitation spectroscopy: the role of phonon-assisted transitions. *Phys. Rev. Lett*. 94:127403
40. Ma Y, Valkunas L, Bachilo S, Fleming GR. 2005. Exciton binding energy in semiconducting single-walled carbon nanotubes. *J. Phys. Chem. Lett*. 109:15671–74
41. Dukovic G, Wang F, Song D, Sfeir MY, Heinz TF, Brus LE. 2005. Structural dependence of excitonic optical transitions and band-gap energies in carbon nanotubes. *Nano Lett*. 5:2314–18
42. Wang Z, Pedrosa H, Krauss T, Rothberg L. 2006. Determination of the exciton binding energy in single-walled carbon nanotubes. *Phys. Rev. Lett*. 96:047403
43. Araujo PT, Doorn SK, Kilina S, Tretiak S, Einarsson E, et al. 2006. Anomalous scaling and a new ratio problem in the optics of carbon nanotubes. *Phys. Rev. Lett.* In press
44. Doorn SK, Heller DA, Barone PW, Usrey ML, Strano MS. 2003. Resonant Raman excitation profiles of individual dispersed SWNTs in solution. *Appl. Phys. A* 78:1147–55
45. Telg H, Maultzsch J, Reich S, Hennrich F, Thomsen C. 2004. Chirality distribution and transition energies of carbon nanotubes. *Phys. Rev. Lett*. 93:177401
46. Sfeir MY, Beetz T, Wang F, Huang L, Huang XMH, et al. 2006. Optical spectroscopy of individual single walled carbon nanotubes of defined chiral structure. *Science* 312:554–56
47. Kane CL, Mele EJ. 2003. Electron interactions and scaling relations for optical excitations in carbon nanotubes. *Phys. Rev. Lett*. 93:197402
48. Ando T. 2006. Effects of valley mixing and exchange on excitons in carbon nanotubes with Aharonov-Bohm flux. *J. Phys. Soc. Jpn*. 75:024707

49. Zaric S, Ostojic GN, Kono J, Shaver J, Moore VC, et al. 2004. Optical signatures of the Aharonov-Bohm phase in single-walled carbon nanotubes. *Science* 304:1129–31
50. Zaric S, Ostojic GN, Shaver J, Kono J, Portugall O, et al. 2006. Excitons in carbon nanotubes with broken time-reversal symmetry. *Phys. Rev. Lett.* 96:016406
51. Zhao H, Mazumdar S. 2004. Electron-electron interaction effects on the optical excitations of semiconducting single-walled carbon nanotubes. *Phys. Rev. Lett.* 93:157402
52. Perebeinos V, Tersoff J, Avouris P. 2005. Radiative lifetime of excitons in carbon nanotubes. *Nano. Lett.* 5:2495–99
53. Mortimer IB, Nicholas RJ. 2006. Role of bright and dark excitons in the temperature dependent photoluminescence of carbon nanotubes. *Phys. Rev. Lett.* In press
54. Son H, Reina Cecco A, Samsonidze GG, Saito R, Jorio A, et al. 2006. Raman characterization of electronic transition energies of metallic single wall carbon nanotubes. *Phys. Rev. B* 74:073406
55. Popov VN. Curvature effects on the structural, electronic and optical properties of isolated single-walled carbon nanotubes within a symmetry-adapted non-orthogonal tight-binding model. *New J. Phys.* 6:17

Annual Review of
Physical Chemistry

Volume 58, 2007

Contents